Langmuir

ARTICLE

pubs.acs.org/Langmuir

Surfactant-Induced Formation of Honeycomb Pattern on Micropipette with Curvature Gradient

Xiaoli Jiang,[†,‡] Tianzhu Zhang,[†,‡] Lina Xu,[†] Changling Wang,[†] Xuefeng Zhou,[†,‡] and Ning Gu*[,†,‡]

[†]Jiangsu Key Laboratory for Biomaterials and Devices, State Key Laboratory of Bioelectronics, School of Biological Science and Medical Engineering, Southeast University, 4 Sipailou, Nanjing 210096, China

[‡]Suzhou Key Lab of Biomedical Materials and Technology, Research Institute of Southeast University in Suzhou, 150 Ren Ai Road, Suzhou Industrial Park, Suzhou 215123, China

Supporting Information

ABSTRACT: Breath figure (BF) process is a facile method to prepare honeycomb structures by dynamic movements of condensed micrometer-sized water droplets at the interface of volatile fluid. Here, we aim to find answers to understand how the BF process occurs on micropipettes with curvature gradient and to understand the role of the surfactant in obtaining honeycomb patterns. Poly (L-lactic acid) (PLLA) chloroform solution with dioleoylphosphatidylethanolamine (DOPE) as surfactant was utilized. It is found that the honeycomb structure formed on the micropipettes changes remarkably with the gradually increased surface curvature. The variation trends of the arrangement and diameter of pores on the micropipettes with the increasing curvature are similar to the different time stages of BF process: smaller and sparse pores formed at higher curvature are similar to those formed at early stage of BF; regular honeycomb patterns formed at lower curvature are similar to those formed at the late stage of BF. Especially, the "semi-coalescence" hemispherical pores strings are found at high curvatures on PLLA−DOPE films, indicating the surfactant-induced coalescence of water droplets in BF process. The differences of drying speed of polymer solvent on micropipette with gradually increased curvatures make the printing of the pores at different BF stages on polymer film possible. These findings not only strongly support the mechanism of BF array formation, but also elucidate the surfactant-induced coalescence.

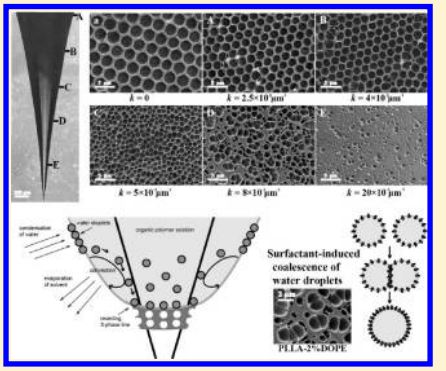

INTRODUCTION

Ordered microporous honeycomb structures have attracted considerable attention due to their wide uses as electronic[1] and photonic[2] materials, catalysts,[3] cell culture substrates,[4,5] etc. The preparation of these structures usually involves photolithography,[6] soft lithography,[7] and templating methods.[8,9] Among these, the breath figure (BF) method represents a simple casting technique for fabricating honeycomb-structured polymer films by in situ condensation of water droplets as templates onto a drying polymer solution.[10] The BF usually takes place in a humid condition. The evaporation of organic solvent decreases the surface temperature and makes water droplets condense on the surface and subsequently grow. After some time, the droplets self-assemble into a well-ordered hexagonal array by thermofluid dynamic movements. As the concentration of the polymer increases with solvent evaporation, the precipitation of the polymer on the interface stabilizes the droplets and prevents coagulation. After complete solvent evaporation, the honeycomb-patterned polymer film is formed with the water droplet array as a template. Finally, a microporous polymer film is obtained after water evaporation.[11−13]

By using BF method, it is possible to control the size and depth of the pores by varying casting conditions like humidity level, concentration of polymer solution, the temperature, the properties of polymers, and so on.[14−17] The water droplet size seems to decrease linearly with the air speed and increasing polymer concentration, while increasing humidity leads to larger water droplets.[18−20] Also, the molecular weight of polymer exerts a decisive influence on honeycomb pores.[21]

However, most of the works are based on the patterning of polymer thin films on flat substrates. The formation of honeycomb structures on nonplanar substrates is significantly less developed, while this might lead to a new class of materials and microstructures. As compared to traditional templating methods, which have limitations that the films are difficult to grow on curved substrates,[22,23] the BF method provides a facile preparation of porous materials on nonplanar substrates. Recently, the example of the fabrication of porous polymer films on nonplanar TEM grids,[24−26] particulate surfaces,[27] bas-relief pattern,[28] various shapes of gratings,[29] and sugar crystal[30] was reported. However, this hierarchic patterning of microporous films by the mentioned works is limited by the particular chemical reaction and complicated synthesis of polymers. Also, the study of the influence of nonplanar substrate on BF structure formation process has been lacking. In fact, the exact mechanism of

Received: January 28, 2011
Revised: March 23, 2011
Published: April 06, 2011

Scheme 1. Schematic Illustration of the Fabrication of Honeycomb-Structured PLLA Film on Glass Micropipettes with Gradually Increasing Curvature by BF Method

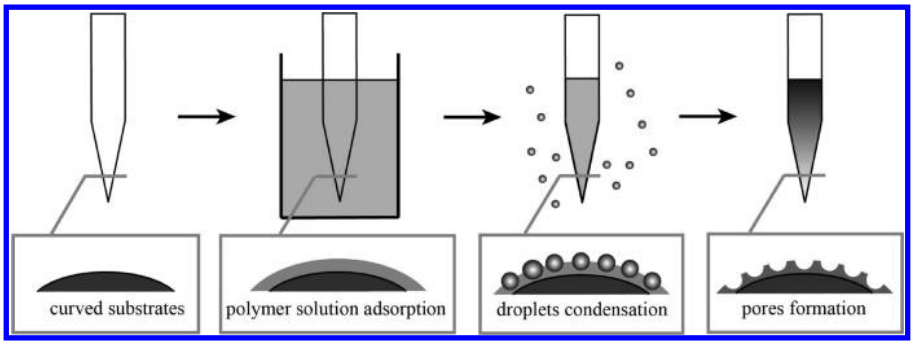

BF formation is still not fully understood, and the mechanism of droplet stabilization is also under debate. Therefore, investigation of the substrate effect on BF process might be helpful to elucidate the mechanisms involved.

Usually, not all kinds of polymers can be utilized for the formation of regular pore arrays by BF method. To date, a range of different polymers have been used to obtain honeycomb-structured films on flat substrates, such as rod−coil block copolymers,[31] block copolymers,[32] conjugated polymers,[16] dendronized polymers,[33] star polymers,[17] and core cross-linked star (CCS) polymers.[27] The restriction of the choice of polymers might limit the applications of BF methods. Like commercially available poly (L-lactic acid) (PLLA), which is one of the most widely used polymeric materials for bone tissue engineering,[34] in most cases, it is difficult to form ordered microporous films by BF method. In this case, a surfactant is essential to stabilize the water droplets. For PLLA, dioleoylphosphatidylethanolamine (DOPE), a naturally derived phospholipid, is reported to be the best choice as the surfactant.[35]

In this work, we aim to investigate the surfactant-induced BF process on glass micropipettes with a curvature gradient. The interesting question is, how does the BF process happen on the micropipette surface? What roles do the curvatures and surfactant play in determining the dynamics and morphology of the growth pattern of droplets? It is our purpose to perform experiments to obtain some preliminary answers to these questions. By casting PLLA solution with different amounts of DOPE on glass micropipettes in a humid condition, the effects of the curvatures and DOPE concentrations on honeycomb pattern formation were studied. The possible mechanisms of the dynamics and interfacial effects of droplets on the micropipettes were also discussed.

EXPERIMENTAL SECTION

Fabrication of Glass Micropipettes. The glass micropipettes were prepared from borosilicate capillary tubes (1.5 mm outer diameter, 1.1 mm inner diameter, Sutter Instruments, Novato, CA) with a P-97 Flaming/Brown micropipette puller (Sutter Instruments, San Rafael, CA). With different parameters of micropipettes puller, glass micropipettes with different tip diameters can be obtained. For this work, the following parameters were used: step 1, Heat 550, Pull 70, Velocity 100, and Time 250; step 2, Heat 540, Pull 70, Velocity 100, and Time 250; step 3, Heat 530, Pull 70, Velocity 100, and Time 250. With these settings, micropipettes with a conical part, having a tip length of about 5.5 mm and minimal diameter of about 10 μm, were obtained.

Formation of Honeycomb-Structured PLLA Films. PLLA (M_W = 100 000, Shandong Institute of Medical Instrument, Shandong, China) was dissolved in chloroform (AR, China National Medicine Corporation Ltd., Shanghai, China) at a concentration of 2 mg/mL. DOPE (≥99.0% (10 mg of phospholipid per mL $CHCl_3$, TLC), Sigma, U.S.) was added into the PLLA solution in concentrations of 2%, 0.5%, or 0.125% by weight based on the weight of PLLA.

The honeycomb-patterned films were prepared by casting the polymer solution at high humid conditions at 25 °C in an experiment setup with controlled temperature and humidity. The schematic and detailed description of the experiment setup is presented in the Supporting Information. Honeycomb-structured PLLA films on flat substrates were prepared by casting PLLA or PLLA−DOPE solution on cover glasses. Microporous PLLA films on glass micropipettes were fabricated as illustrated in Scheme 1. First, after being washed with water and then dried, the tip of the micropipette was immersed into the polymer solution. After several seconds, the pipette was pulled out of the polymer solution slowly and then dried in a humid condition (RH = 90%) at 25 °C. The pulling speed of the glass micropipette was coarsely controlled by a lift table in the temperature- and humidity-controlled setup as illustrated in the Supporting Information. After complete evaporation of the solvent, the polymer film with the porous pattern was formed on the micropipet. Experiments were run in triplicate, repeated at least three separate times.

Characterization. The morphology of the microporous PLLA films on flat substrates and the glass micropipettes was observed directly by using optical microscopy (Axiovert 200, Zeiss). Also, a Zeiss Ultra Plus field emission scanning electron microscope (SEM) with InLens capabilities, using nitrogen gas and ultrahigh-resolution BSE imaging, was used to study the surface morphology of nonconductive samples. Therefore, the glass micropipettes covered with honeycomb-structured PLLA film can be directly observed under SEM without conducting coating. The cylindrical end of the micropipette was attached to the SEM sample stage by conductive adhesives, and the morphology of the polymer film on micropipette was observed with an operating voltage of 1 kV under ultrahigh vacuum conditions.

A quantitative evaluation of the order of honeycomb patterns was made by using the Voronoi polygon construction.[36−38] The SEM images were processed and analyzed by the freeware image analysis software called ImageJ. The SEM images were first elaborated to obtain black and white images at high resolution. The pores were then automatically identified, and the area and circularity were evaluated. The Voronoi tessellation of the images and the calculation of the entropy of the pattern were performed with the MATLAB software.

RESULTS AND DISCUSSION

The conical section of a glass micropipette with a minimal diameter of about 10 μm is characterized under optical microscopy as shown in Figure 1. After the BF process, the micropipette surface is covered with a layer of microporous PLLA film. Five sections of the micropipette with different curvatures are chosen for the observation of the film morphologies. The cross section of

the micropipette is a disk; hence the surface curvature k equals $1/R$. The surface curvatures k, which refer to the cross sections from A to E (as noted on the micropipette in Figure 1), are 2.5×10^{-3}, 4×10^{-3}, 5×10^{-3}, 8×10^{-3}, and 20×10^{-3} μm^{-1}, respectively.

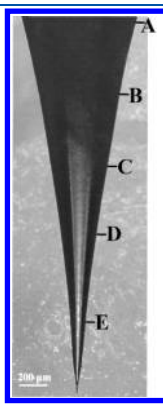

Section	Curvature (k = 1/R) (10^{-3} μm^{-1})
A	2.5
B	4.0
C	5.0
D	8.0
E	20.0

Figure 1. Characterization of the micropipettes under optical microscopy. Five sections (A−E) of the micropipette with different curvatures are chosen for the observation of the film morphologies. The corresponding curvatures of sections A−E are listed in the table.

First, PLLA−2%DOPE solution (2 mg/mL PLLA solution with 2% DOPE based on the weight of PLLA) was used to cast on cover glasses or micropipettes to investigate the influence of surface curvature on the formation of honeycomb-structured films. The SEM images of porous PLLA−2%DOPE film on different curvature were taken. The analysis of the pore size (average diameter, AD) and pore size distribution has been performed, using the image analysis software (ImageJ). ImageJ is able to identify each pore and provide its area information. The AD is calculated from the area (area = $\pi(AD/2)^2$). Results and corresponding SEM images are presented in Figure 2. On a flat substrate, a uniform honeycomb structure is clearly observed as shown in Figure 2a. The pores are hexagonally close-packed, and the AD is 2.637 ± 0.120 μm. The morphology of PLLA film formed on the glass micropipette changes at different sections (Figure 2A−E). When casting at $k = 2.5 \times 10^{-3}$ μm^{-1} (Figure 2A), the pores are not fully hexagonally close-packed, and the AD reduces to 1.879 ± 0.121 μm. With the increase of surface curvature ($k = 4 \times 10^{-3}$ μm^{-1}), the honeycomb structure becomes more disordered, and the AD continuously reduces to 1.774 ± 0.212 μm as shown in Figure 2B. At the section of $k = 5 \times 10^{-3}$ μm^{-1} (Figure 2C), the shapes of the pores turn to irregular sphere, and the calculated AD turns to 0.923 ± 0.136 μm. When the curvature increases to 8×10^{-3} μm^{-1} (Figure 2D), the pores

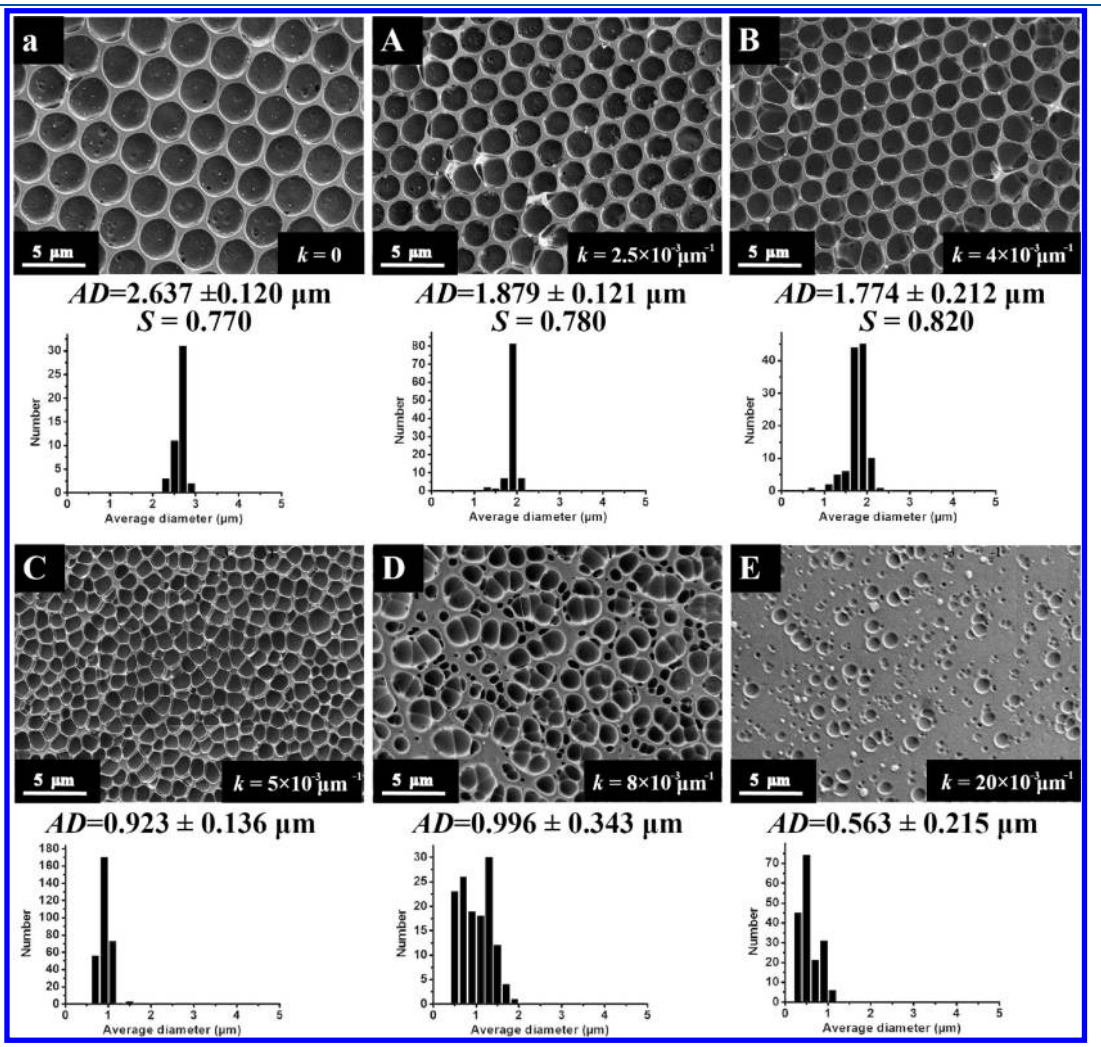

Figure 2. SEM images, average diameters (AD), entropy (S), and size distributions of pores on PLLA−2%DOPE films cast at 90% RH on (a) cover glasses and (A−E) glass micropipettes taken at different sections with increasing curvature.

dx.doi.org/10.1021/la200375t |*Langmuir* 2011, 27, 5410–5419

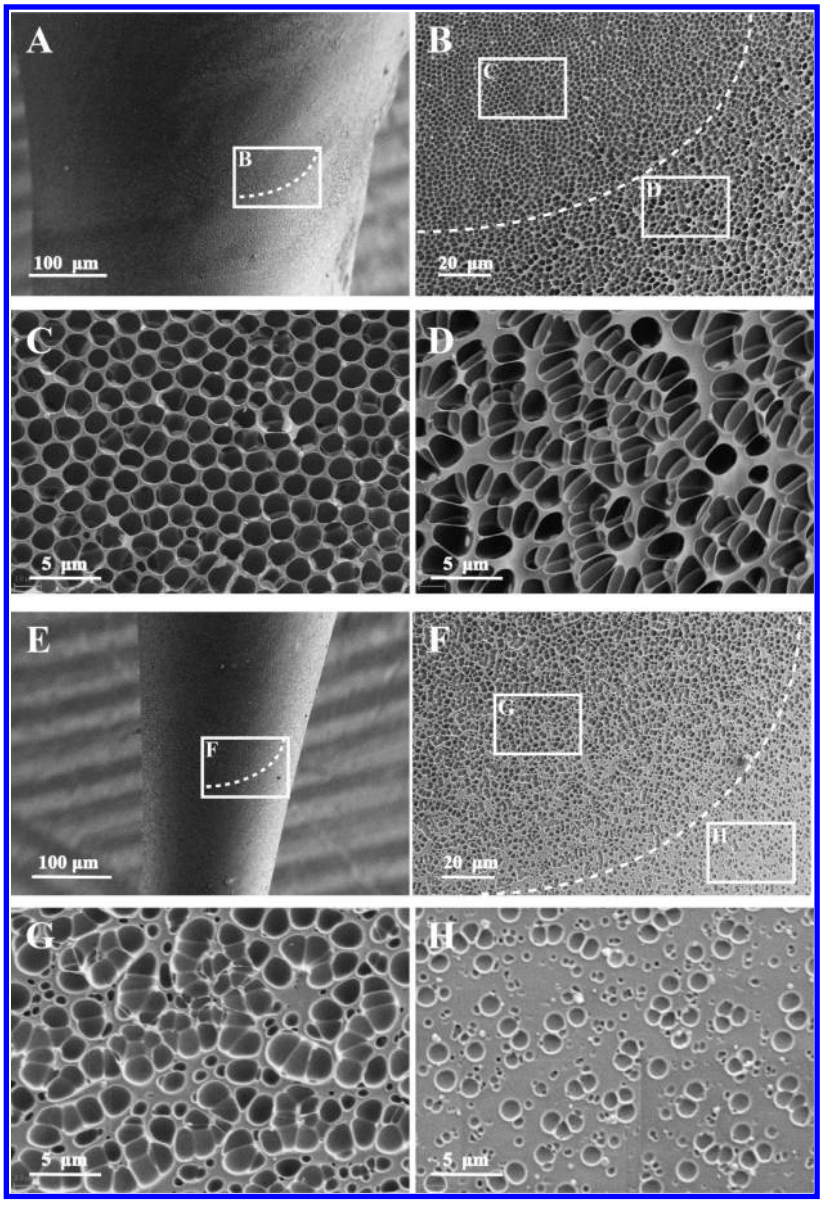

Figure 3. SEM images of PLLA−2%DOPE cast on micropipettes show two transition zones of the arrangement and shapes of pores. (A−D) The transition zone at the curvature of around $(4-5) \times 10^{-3}\ \mu m^{-1}$ represents the change between honeycomb structure and irregular hemispherical pores. (E,F) The transition zone at the curvature of around $(10-15) \times 10^{-3}\ \mu m^{-1}$ shows the change between irregular hemispherical pores and random dispersed spherical pores.

become irregular hemispherical, and several pores are close to each other, forming pore strings. The length of the irregular spherical pores increases to around 3 μm, and the calculated AD increases to $0.996 \pm 0.343\ \mu$m. Next, at $k = 20 \times 10^{-3}\ \mu m^{-1}$ (Figure 2E), the shape of the pores returns to sphere, and the pore sizes continue to decrease (AD = $0.563 \pm 0.215\ \mu$m) with the increase of surface curvature. Meanwhile, the coverage of pores reduces. As far as pore size distribution is concerned, porous patterns obtained on the flat substrate and on section A−B on the micropipette present a monomodal distribution. On the contrary, the PLLA film formed on section C−E on the micropipette shows a multimodal distribution.

The degree of order can be quantitatively evaluated by construction of Voronoi polygons.[36] The analysis of Voronoi constructions has been performed for the most regular honeycomb patterns (Figure 2a,A,B) as shown in the Supporting Information. The probabilities of pores with four-, five-, six-, and seven-nearest neighbors (P_4, P_5, P_6, and P_7) give the conformational entropy ($S = -\Sigma P_n \ln P_n$).[39] The lowest S of conformation, that is, maximum order of honeycomb array, was obtained for PLLA−2%DOPE film on flat substrate (S = 0.770). Higher S values, that is, less ordered arrays, were obtained for PLLA−2%DOPE film cast on the micropipette at section A ($k = 2.5 \times 10^{-3}\ \mu m^{-1}$, $S = 0.780$) or B ($k = 4 \times 10^{-3}\ \mu m^{-1}$, $S = 0.820$). These values are all significantly less than the value 1.71, which is reported for the random distribution.[36] The results quantitatively bring out that the observed patterns are fairly highly ordered. Attempts to find a quantitative of the porous patterns on higher curvatures were unsuccessful.

It is interesting to notice that there are two transition zones of the arrangement and shapes of pores. The first one is at the curvature of around $(4-5) \times 10^{-3}\ \mu m^{-1}$, as shown in Figure 3A−D. There is a segment of a curved transition line between honeycomb structure and irregular hemispherical pores. The second transition zone is

dx.doi.org/10.1021/la200375t |*Langmuir* 2011, 27, 5410–5419

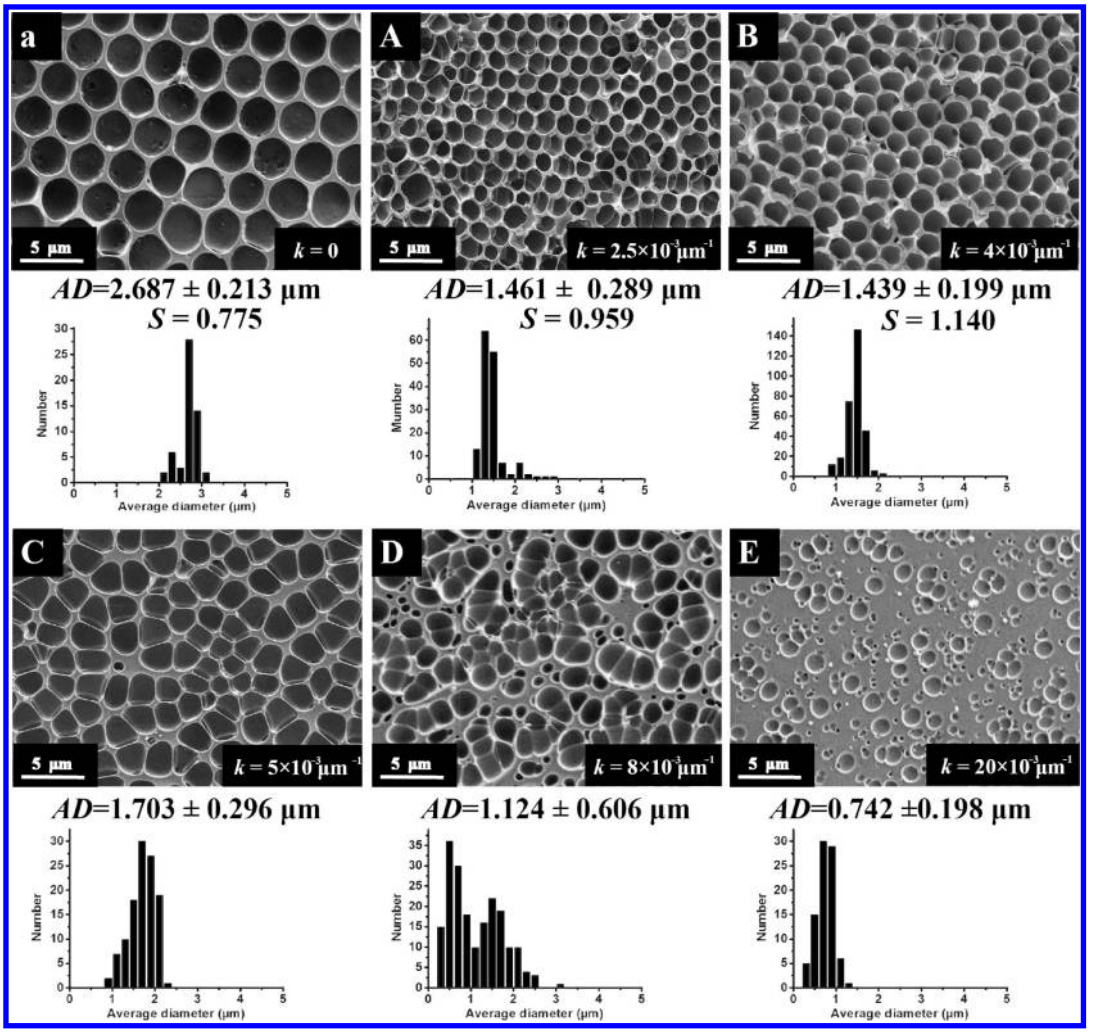

Figure 4. SEM images, average diameters (AD), entropy (S), and size distributions of pores on of PLLA−0.5%DOPE films cast at 90% RH on (a) cover glasses and (A−E) glass micropipettes taken at different sections with increasing curvature.

at the curvature of around $(10-15) \times 10^{-3}\ \mu m^{-1}$ as shown in Figure 3E,F, where there is also a curved transition line between irregular hemispherical pores and randomly dispersed spherical pores. The curved line might be caused by the curvature of the conical section of the pipette. Also, the gradually changed curvature on a single substrate is essential for the observation of the transition zones.

The effects of DOPE concentration on the honeycomb structure formation on curved substrate were evaluated. PLLA−0.5% DOPE solution (2 mg/mL PLLA solution with 0.5% DOPE based on the weight of PLLA) and PLLA solution without DOPE were cast on the micropipettes, respectively. Figure 4 represents the SEM images and size distributions of PLLA−0.5%DOPE films on cover glasses or the micropipettes. It can be found that the variations of arrangement and shapes of pores on PLLA−0.5% DOPE are similar to those on PLLA−2%DOPE. However, size distributions of the PLLA−0.5%DOPE porous film are broader. Also, as compared to the pores of PLLA−2%DOPE at the same curvature, pores on PLLA−0.5%DOPE at higher curvatures ($k = 2.5 \times 10^{-3}$ and $4 \times 10^{-3}\ \mu m^{-1}$) are more disordered (at section A, $S = 0.959$; at section B, $S = 1.140$) (Voronoi constructions of Figure 4a,A,B are shown in the Supporting Information). The results are understandable because the lower concentration of surfactant reduces the ability of droplet stabilization. Lower concentration of DOPE (PLLA−0.125%DOPE) was also examined (Supporting Information) and showed that the pores on the micropipette also change with the curvature as with the other two concentrations of DOPE. The difference is that the hemispherical pores appear at lower curvature ($k = 5 \times 10^{-3}\ \mu m^{-1}$) as compared to those of PLLA−0.5%DOPE and PLLA−2%DOPE.

Figure 5 shows SEM images of PLLA films without DOPE casting at the same conditions of PLLA−DOPE. Usually, it is difficult for commercially available PLLA to form ordered microporous films by BF method. As can be seen in Figure 5a, on flat substrate, an irregular pore pattern with a pore size ranging from about 10 to 1 μm is formed. Most of the pores have the AD of $2.681 \pm 2.212\ \mu$m, while a few of them are about 10 μm. There is also a subpattern of smaller pores in the layer beneath the first layer of pores on the flat substrate. However, this double porous pattern disappears on curved substrate (Figure 5A−E), which might be caused by the reduced amount of polymer solution adsorbed on the micropipette. Without DOPE, the porous PLLA film on the micropipette is quite disordered so that the Voronoi polygon is not able to be constructed. However, the size distribution is improved to some extent that larger and smaller pores disappear as compared to that on flat substrate. Narrower size distributions are obtained at higher curvatures. The pore sizes

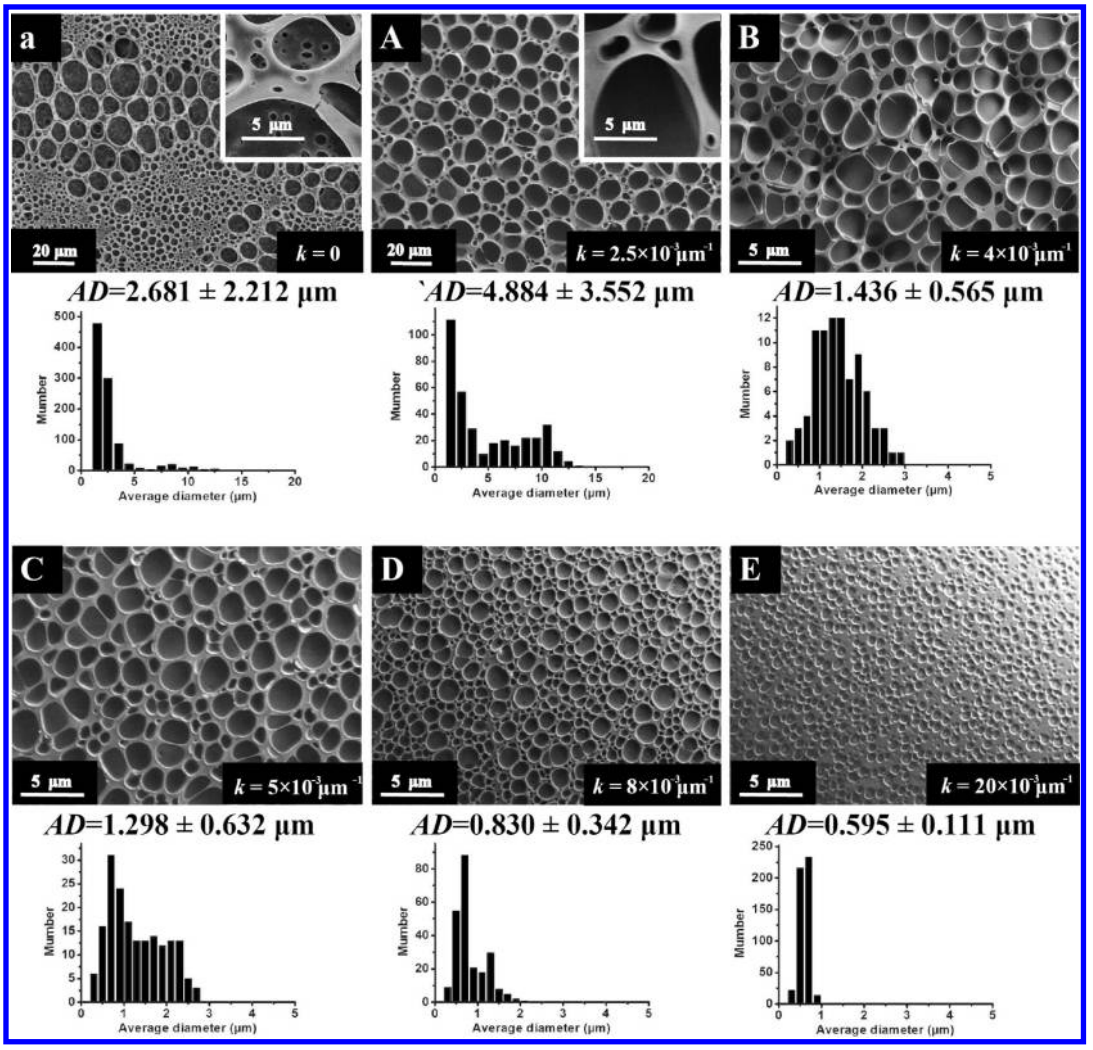

Figure 5. SEM images, average diameters (AD), and size distributions of pores on PLLA films without DOPE cast at 90% RH on (a) cover glasses and (A−E) glass micropipettes taken at different sections with increasing curvature.

also continue to decrease with the increase of surface curvature as PLLA−DOPE. The shapes of the pores are irregular spherical before the curvature of $8 \times 10^{-3}\ \mu m^{-1}$ and spherical after that. The hemispherical shapes and the pores strings, which are observed on PLLA−DOPE, are not obviously found on PLLA films.

The average diameters of the pores on polymer films cast on flat surfaces and the micropipettes from PLLA with different DOPE concentration are summarized in Figure 6A. The AD basically decreases with the increase of curvature in all three groups. The distribution of pores (error bar of the diameter) mainly becomes broader for PLLA−2%DOPE and PLLA−0.5% DOPE and narrower for PLLA−0%DOPE with the increase of curvature. In general, PLLA−2%DOPE represents a narrower size distribution than does PLLA−0.5%DOPE, and both of them reach the broadest distribution at $k = 5 \times 10^{-3}\ \mu m^{-1}$. The shapes of the pores were analyzed and expressed as circularity. The circularity is a measure of the compactness of a shape. A circle is the most compact shape with the circularity of 1, so the more compact a shape is, the more closely it resembles a circle. The summary of the circularity of pores on films in the three groups is illustrated in Figure 6B. In general terms, pores show a high circularity at lower curvatures for the three groups. The shapes of the pores then turn irregular and get the lowest circularity at $k = 8 \times 10^{-3}\ \mu m^{-1}$ for PLLA−DOPE and at $k = 5 \times 10^{-3}\ \mu m^{-1}$ for PLLA. With the increase of curvature, the error bar of circularity increases in the PLLA−DOPE group and remains at the same level in the PLLA group. The results of the AD and circularity of the three groups illustrate that the curvature effect on the diameters are greater in the PLLA group, while the effect on the shapes is greater in the PLLA−DOPE groups. The concentration of DOPE affects the distribution of pore size and the order of the pores array (according to the *S*).

Scheme 1 illustrates, schematically, how the BF process could occur on micropipette with gradually increasing curvature. By immersion in $CHCl_3$ solution of PLLA, the glass micropipette is covered with a thin layer of polymer solution. This solution on curved substrate is exposed to a humid condition. The rapid evaporation of the volatile solvent causes a decrease in the surface temperature. The subsequent condensation of water from the moist environment onto the solution surface results in the presence of isolated water droplets floating on the curved organic surface. The density of water droplets on the surface increases simultaneously with the growth of the existing water droplets.[40] PLLA or DOPE in the solution precipitates around these water

dx.doi.org/10.1021/la200375t |*Langmuir* 2011, 27, 5410–5419

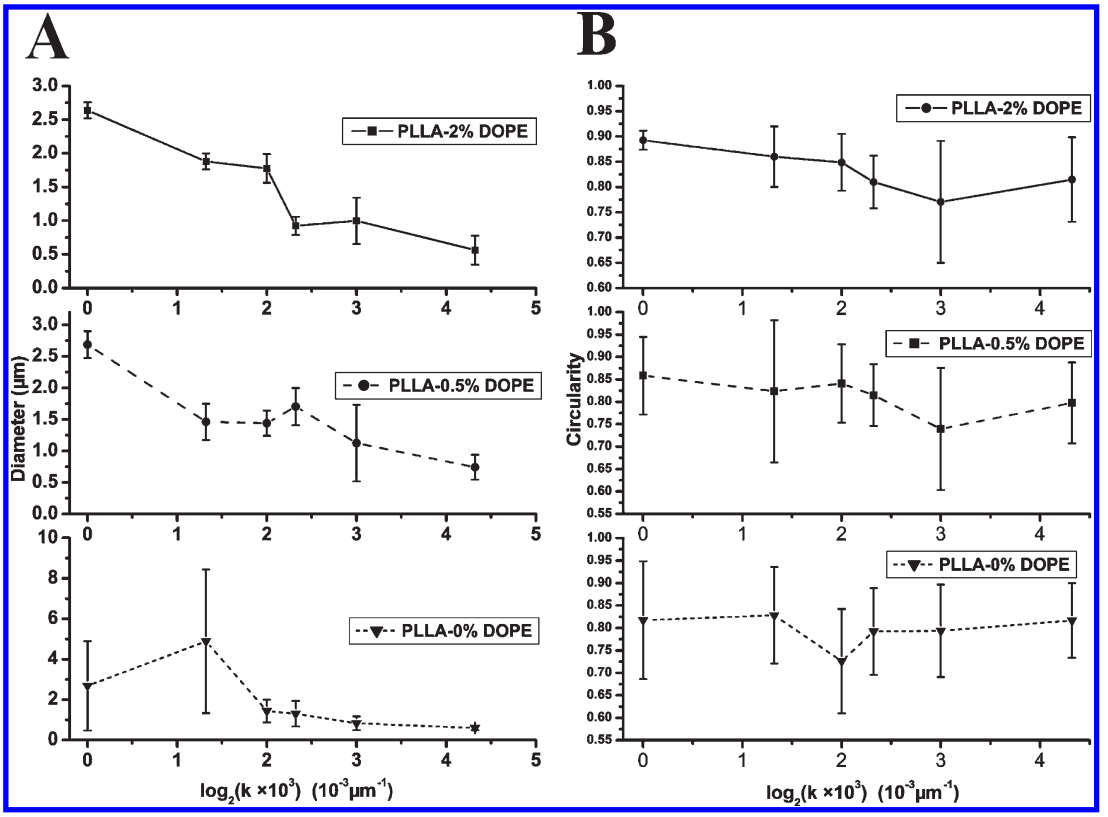

Figure 6. The summary of (A) average diameters and (B) the circularity of pores on porous films cast on flat surfaces and the micropipettes from PLLA with different DOPE concentration.

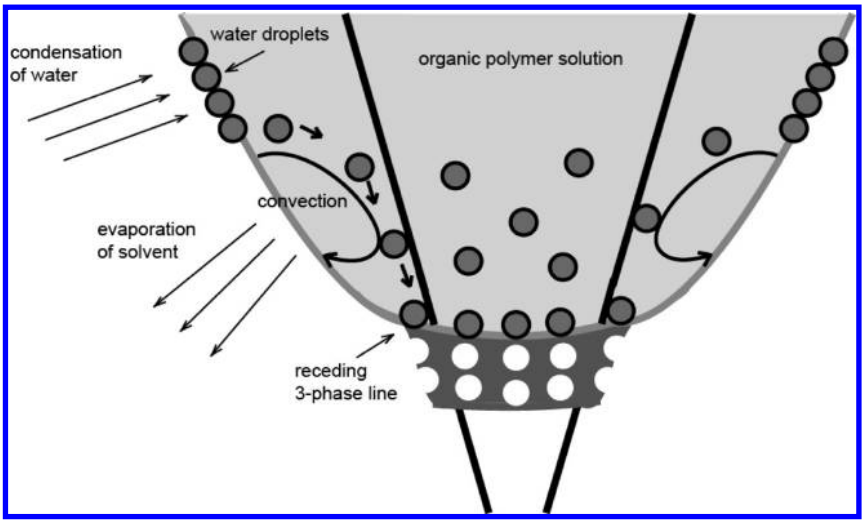

Figure 7. Formation mechanism of honeycomb structure on micropipettes.

droplets, stabilizing them from coalescence. With complete evaporation of the solvent and water droplets, the porous film will be left on the curved substrate.

There are basically there stages of BF process in chronological order: (1) nucleation and growth of droplets; (2) coalescence of droplets; and (3) arrangement of droplets into hexagonal array. It is interesting to notice that the variation trend of the porous film formed on the micropipette at different curvatures is similar to that of honeycomb film at different time periods in the BF process: at early stage of BF, the condensed droplets are small in size and randomly arranged; at later stage of BF, droplets are more closed-packed and self-organize into hexagonal array. This can be explained by the mechanism for the arrangement of droplets on the micropipette, which is illustrated in Figure 7. The honeycomb structure forms by the dynamic movement of the water droplets. With the evaporation of $CHCl_3$ solution, water droplets nucleate on the surface and subsequently grow. The amount of solution adsorbed on the pinpoint of the micropipette is less as compared to that on the cylindrical part, so the three-phase line (solution−air−substrate) is supposed to start from the peak of the micropipette, which dries fastest. Next, the

dx.doi.org/10.1021/la200375t |*Langmuir* 2011, 27, 5410–5419

three-phase line moves over the array of water droplets and moves toward the cylindrical part of the micropipette. At the peak of the micropipette, when the solvent just begins to evaporate, only a few droplets are condensed on the solvent surface, resulting in the formation of sparse micropores and low surface coverage. As evaporation of the solvent proceeded, rafts of noncoalescing droplets form and organize on the surface into a hexagonally ordered array by the thermocapillary effect combined with Marangoni convection.[41] Therefore, the pore arrays formed later on the micropipette at smaller curvatures are more ordered.

The mechanism of BF is based on the dynamic movement of droplets at the interface. The direct evidence to support this theory is the real-time observation with microscopy.[42] However, due to the limit of the microscopy magnification, the detail of the process (like the coalescence of droplets) is lacking. Usually, the pore array at different stages cannot be preserved on the polymer films. Casting polymer solution on the micropipette is able to solve this problem. The gradually increased curvatures cause the differences of solution amount on different sections of the micropipette, so the differences of corresponding drying speed might be amplified. The pinpoint of the micropipettes dries much faster than that of the flat substrate, which makes the printing of the pores at BF early stage on polymer film possible. It is helpful for better understanding the dynamic movement of droplets and the development process of BF.

The variation of the pores shapes on the micropipettes might be caused by the surfactant-induced coalescence of droplets. The sizes of the pores are mainly determined by the sizes of the condensed water droplets. The droplet diameter a is observed to grow with time according to $a \propto bt^{1/3}$, where b is a function of the velocity of the airflow and the surface temperature.[13] The condensation is governed by the growth of individual droplets and the coalescence of droplets when they touch. When in a surfactant (DOPE)-stabilized system, the coalescence also depends on the surfactant concentrations.[43,44] The initially formed drops (which are not covered with complete surfactant layers) coalesce with each other until their surfaces become completely covered and protected by a dense layer of surfactant.[45,46] DOPE-stabilized coalescence is illustrated in Figure 8A. The "hemi-coalescence" pores with irregular hemispherical shapes are found on PLLA films with a different amount of DOPE at the curvature of 8×10^{-3} μm^{-1} (Figure 8B). The mean drop size increases with the decrease of DOPE concentration. In the case of PLLA film without DOPE, the irregular hemispherical pores disappear due to the lack of stabilizer. The observation of the "hemi-coalescence" phenomenon is beneficial for better understanding the stabilized mechanism of the surfactant.

Besides the surfactant concentration, the coalescence of the droplets is also affected by the lateral capillary force between droplets floating on the fluid interface. The interaction effects of droplets on flat or curved substrate are illustrated in Figure 9. There are two kinds of forces between two identical droplets of a radius R separated by a center-to-center distance L: flotation force (by gravity) and immersion force (by wetting).[47] The flotation force is negligible for droplets smaller than 5−10 μm. The lateral capillary force can be calculated by eq 1.[48,49]

$$F_i = 2\pi\sigma Q_1 Q_2 L^{-1} \quad (1)$$

where σ is surface tension, and for the two droplets at the same size, $Q_1 = Q_2 = r \sin \psi$, where r is the radius of contact lines and ψ is the meniscus slope angle (Figure 9A). In the case of the

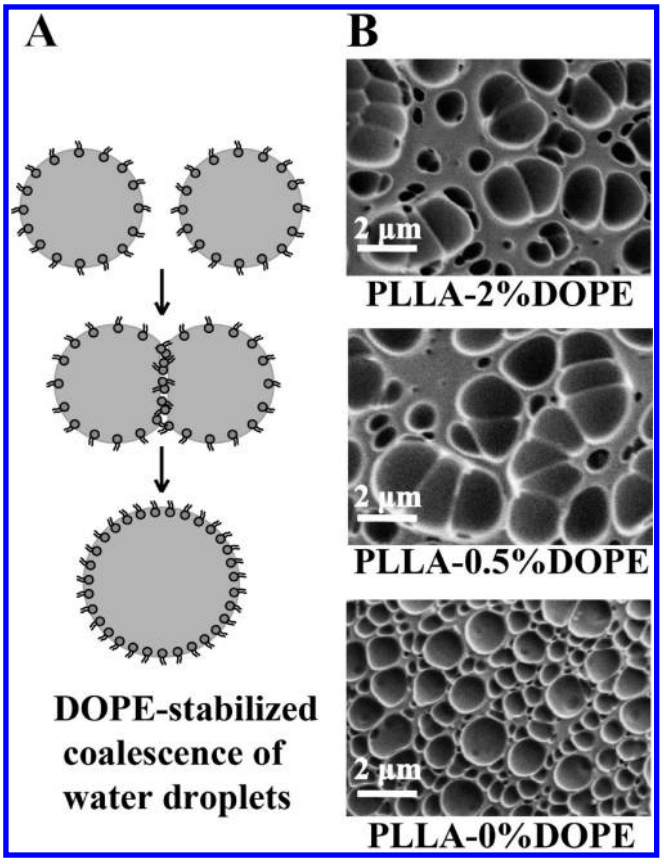

Figure 8. (A) Schematic illustration of DOPE-stabilized coalescence of water droplets. (B) The experimental observations of the coalescence on PLLA−2%DOPE, PLLA−0.5%DOPE, and PLLA−0%DOPE films at the curvature of 8×10^{-3} μm^{-1}, respectively.

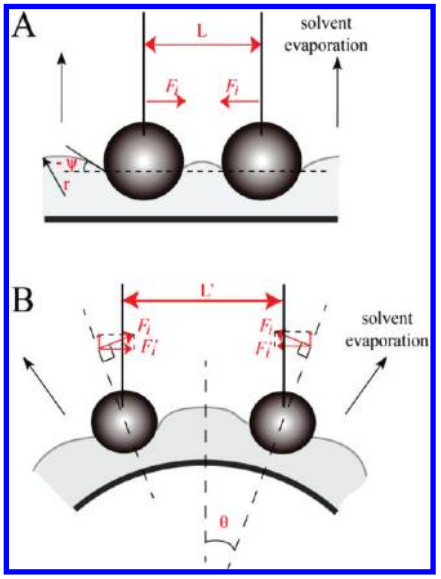

Figure 9. Schematic illustration of capillary force between two droplets on (A) flat substrate and (B) curved substrate.

interaction between droplets attached to a curved interface, the meniscus slope angle ψ decreases, and $F_i' = \sin \theta F_i$ (θ is the excursion angle of droplet on a curved substrate, which increases with substrate curvatures) (Figure 9B). So the lateral capillary

dx.doi.org/10.1021/la200375t |*Langmuir* 2011, 27, 5410–5419

force between two droplets decreases due to the increase of curvature. Thus the droplets tend to be separated from each other rather than coagulated as compared to those on flat substrates.

CONCLUSION

Patterning of honeycomb structure on evaporating PLLA–DOPE solution on glass micropipettes with gradually increasing surface curvature is studied. The arrangement and sizes of pores may change from part to part on the micropipette. For PLLA–DOPE, at low surface curvatures, the pores are mostly hexagonal packed as those on flat substrates; at high surface curvatures, the pores become irregular shaped and more randomly dispersed. It is interesting to notice that at high curvatures, several of the pores are extremely close to each other, forming "semi-coalescence" hemispherical pores strings. The results of the AD and circularity of the PLLA with different DOPE concentration illustrate that the curvature effect on the diameters is greater in PLLA group, while the effect on the shapes is greater in PLLA–DOPE groups. The concentration of DOPE affects the distribution of pore size and the order of the pores array. The variation of the pores on the micropipette at different sections is similar to that of BF process at different times. The differences of drying speed might be amplified by the curvature gradient, which makes it possible to preserve pores array at different stages of BF process on polymer film. The dynamics of droplets coalescence and the interactions between droplets affect the shape of DOPE-stabilized droplets. The utilization of micropipettes as substrates for casting of polymer porous films via BF method is beneficial for better understanding the dynamic movement of droplets and the development process of BF. Also, the "hemi-coalescence" structures in PLLA–DOPE groups provide direct evidence of the surfactant-induced coalescence of water droplets. The effect of curvature on porous films formed in BF process also opens a new route for controlling the sizes and shapes of pores. The applicability of the honeycomb-patterned films can be expanded by casting on nonplanar substrates, such as substrates for microelectrical devices and biomedical devices.

ASSOCIATED CONTENT

Supporting Information. Experiment setup with controlled temperature and humidity, setup for controlling the pulling speed, Voronoi constructions of Figures 2a,A,B and 4a, A,B, and PLLA–0.125%DOPE casting on cover glasses and the micropipettes. This material is available free of charge via the Internet at http://pubs.acs.org.

AUTHOR INFORMATION

Corresponding Author

*Phone: +86-(0)25-83272460. Fax: +86-(0)25-83272476. E-mail: guning@seu.edu.cn.

ACKNOWLEDGMENT

We acknowledge the support of the National Basic Research Program of China (2011CB933500), the National Natural Science Foundation of China (NSFC, 60725101, 50872021), the International Cooperation Program awarded by MOST (the Ministry of Science and Technology) of China (2008DFA51180), the National Science Foundation of Jiangsu province in China (SBE201077305, BK2009592), and the Qing Lan Project.

REFERENCES

(1) Zhang, Y. L.; Zha, S. W.; Liu, M. L. *Adv. Mater.* **2005**, *17*, 487.
(2) Walheim, S.; Schaffer, E.; Mlynek, J.; Steiner, U. *Science* **1999**, *283*, 520.
(3) Tanev, P. T.; Chibwe, M.; Pinnavaia, T. J. *Nature* **1994**, *368*, 321.
(4) Beattie, D.; Wong, K. H.; Williams, C.; Poole-Warren, L. A.; Davis, T. P.; Barner-Kowollik, C.; Stenzel, M. H. *Biomacromolecules* **2006**, *7*, 1072.
(5) Chaudhuri, J. B.; Davidson, M. G.; Ellis, M. J.; Jones, M. D.; Wu, X. J. *Macromol. Symp.* **2008**, *272*, 52.
(6) Jonas, U.; del Campo, A.; Kruger, C.; Glasser, G.; Boos, D. *Proc. Natl. Acad. Sci. U.S.A.* **2002**, *99*, 5034.
(7) Xia, Y. N.; Whitesides, G. M. *Angew. Chem., Int. Ed.* **1998**, *37*, 551.
(8) Holland, B. T.; Blanford, C. F.; Stein, A. *Science* **1998**, *281*, 538.
(9) Imhof, A.; Pine, D. J. *Nature* **1997**, *389*, 948.
(10) Bunz, U. H. F. *Adv. Mater.* **2006**, *18*, 973.
(11) Widawski, G.; Rawiso, M.; François, B. *Nature* **1994**, *369*, 387.
(12) Pitois, O.; François, B. *Eur. Phys. J. B* **1999**, *8*, 225.
(13) Pitois, O.; François, B. *Colloid Polym. Sci.* **1999**, *277*, 574.
(14) Englert, B. C.; Scholz, S.; Leech, P. J.; Srinivasarao, M.; Bunz, U. H. F. *Chem.-Eur. J.* **2005**, *11*, 995.
(15) Hernandez-Guerrero, M.; Davis, T. P.; Barner-Kowollik, C.; Stenzel, M. H. *Eur. Polym. J.* **2005**, *41*, 2264.
(16) Song, L.; Bly, R. K.; Wilson, J. N.; Bakbak, S.; Park, J. O.; Srinivasarao, M.; Bunz, U. H. F. *Adv. Mater.* **2004**, *16*, 115.
(17) Stenzel-Rosenbaum, M. H.; Davis, T. P.; Fane, A. G.; Chen, V. *Angew. Chem., Int. Ed.* **2001**, *40*, 3428.
(18) Srinivasarao, M.; Collings, D.; Philips, A.; Patel, S. *Science* **2001**, *292*, 79.
(19) Peng, J.; Han, Y. C.; Yang, Y. M.; Li, B. Y. *Polymer* **2004**, *45*, 447.
(20) Stenzel, M. H. *Aust. J. Chem.* **2002**, *55*, 239.
(21) Xu, Y.; Zhu, B. K.; Xu, Y. Y. *Polymer* **2005**, *46*, 713.
(22) Bang, J.; Kim, S. H.; Drockenmuller, E.; Misner, M. J.; Russell, T. P.; Hawker, C. J. *J. Am. Chem. Soc.* **2006**, *128*, 7622.
(23) Drockenmuller, E.; Li, L. Y. T.; Ryu, D. Y.; Harth, E.; Russell, T. P.; Kim, H. C.; Hawker, C. J. *J. Polym. Sci., Part A: Polym. Chem.* **2005**, *43*, 1028.
(24) Connal, L. A.; Qiao, G. G. *Adv. Mater.* **2006**, *18*, 3024.
(25) Connal, L. A.; Vestberg, R.; Gurr, P. A.; Hawker, C. J.; Qiao, G. G. *Langmuir* **2008**, *24*, 556.
(26) Connal, L. A.; Vestberg, R.; Hawker, C. J.; Qiao, G. G. *Adv. Funct. Mater.* **2008**, *18*, 3315.
(27) Connal, L. A.; Qiao, G. G. *Soft Matter* **2007**, *3*, 837.
(28) Ohzono, T.; Nishikawa, T.; Shimomura, M. *J. Mater. Sci.* **2004**, *39*, 2243.
(29) Park, J. S.; Lee, S. H.; Han, T. H.; Kim, S. O. *Adv. Funct. Mater.* **2007**, *17*, 2315.
(30) Li, L.; Zhong, Y. W.; Gong, J. L.; Li, J.; Chen, C. K.; Zeng, B. R.; Ma, Z. *Soft Matter* **2011**, *7*, 546.
(31) Hayakawa, T.; Horiuchi, S. *Angew. Chem., Int. Ed.* **2003**, *42*, 2285.
(32) de Boer, B.; Stalmach, U.; Nijland, H.; Hadziioannou, G. *Adv. Mater.* **2000**, *12*, 1581.
(33) Cheng, C. X.; Tian, Y.; Shi, Y. Q.; Tang, R. P.; Xi, F. *Langmuir* **2005**, *21*, 6576.
(34) Burg, K. J. L.; Porter, S.; Kellam, J. F. *Biomaterials* **2000**, *21*, 2347.
(35) Fukuhira, Y.; Kitazono, E.; Hayashi, T.; Kaneko, H.; Tanaka, M.; Shimomura, M.; Sumi, Y. *Biomaterials* **2006**, *27*, 1797.
(36) Limaye, A. V.; Narhe, R. D.; Dhote, A. M.; Ogale, S. B. *Phys. Rev. Lett.* **1996**, *76*, 3762.
(37) Park, M. S.; Kim, J. K. *Langmuir* **2004**, *20*, 5347.
(38) Ferrari, E.; Fabbri, P.; Pilati, F. *Langmuir* **2011**, *27*, 1874.
(39) Steyer, A.; Guenoun, P.; Beysens, D.; Knobler, C. M. *Phys. Rev. B* **1990**, *42*, 1086.
(40) Karthaus, O.; Maruyama, N.; Cieren, X.; Shimomura, M.; Hasegawa, H.; Hashimoto, T. *Langmuir* **2000**, *16*, 6071.

(41) Adachi, E.; Dimitrov, A. S.; Nagayama, K. *Langmuir* **1995**, *11*, 1057.
(42) Barrow, M. S.; Jones, R. L.; Park, J. O.; Srinivasarao, M.; Williams, P. R.; Wright, C. J. *Spectrosc. Int. J.* **2004**, *18*, 577.
(43) Golemanov, K.; Tcholakova, S.; Kralchevsky, P. A.; Ananthapadmanabhan, K. P.; Lips, A. *Langmuir* **2006**, *22*, 4968.
(44) Tcholakova, S.; Denkov, N. D.; Sidzhakova, D.; Ivanov, I. B.; Campbell, B. *Langmuir* **2003**, *19*, 5640.
(45) Arditty, S.; Whitby, C. P.; Binks, B. P.; Schmitt, V.; Leal-Calderon, F. *Eur. Phys. J. E* **2003**, *11*, 273.
(46) Arditty, S.; Schmitt, V.; Giermanska-Kahn, J.; Leal-Calderon, F. *J. Colloid Interface Sci.* **2004**, *275*, 659.
(47) Paunov, V. N.; Kralchevsky, P. A.; Denkov, N. D.; Nagayama, K. *J. Colloid Interface Sci.* **1993**, *157*, 100.
(48) Kralchevsky, P. A.; Nagayama, K. *Langmuir* **1994**, *10*, 23.
(49) Danov, K. D.; Kralchevsky, P. A.; Naydenov, B. N.; Brenn, G. *J. Colloid Interface Sci.* **2005**, *287*, 121.